SOLAR RADIATION PROJECTIONS DERIVED FROM GLOBAL CLIMATE MODELS (part of CES deliverable D2.4)

Kimmo Ruosteenoja[1] *and Jouni Räisänen*[2]

[1]Finnish Meteorological Institute, P.O.Box 503, FI-00101, Helsinki, Finland
Email suffix: @fmi.fi

[2]Department of Physical Sciences, P.O.Box 48, FI-00014 University of Helsinki, Finland
Email suffix: @helsinki.fi

16 September 2009

In the future, changes in incident solar radiation are of crucial importance for the conditions of solar energy production. Furthermore, the need for electricity in outdoor and indoor illumination is affected by the availability of solar radiation, especially in late autumn and early winter when light is scant.

In this survey, we compile projections for solar radiation, especially focussing on the Nordic area and the period 2020-2049. Projections are based on simulations performed with 18 global climate models under the SRES A1B, A2 and B1 greenhouse gas scenarios.

To facilitate reading the report, only the most essential diagrams and maps are included in the main text, additional material being positioned in the appendix.

1 MODELLED SOLAR RADIATION DATA

The quantity examined is incident solar radiation (also termed global radiation), i.e., the sum of the direct and diffuse solar radiation. The quantity can be expressed in W/m^2 or MJ/m^2 per time unit. In this account, changes in incident radiation are viewed both in absolute[1] and percentage terms.

Model output data were downloaded from the CMIP3 data archive. There were a few models for which the simulation for one of the three scenarios was missing; in those cases, surrogate simulations were created applying a pattern-scaling technique (Ruosteenoja et al., 2007).

Solar radiation simulations were available for all the 19 models that were employed by Räisänen and Ruosteenoja (2008) in composing temperature and precipitation projections for the CES project. The models were listed in their Table 2.1, accompanied by a brief discussion about the properties of the models in the text. Unfortunately, one of those models, the Australian CSIRO-MK3.0, proved to produce unrealistic simulations for northern areas during the darkest winter months, and inclusion of this model in the

[1]The absolute megajoule-unit changes were calculated directly from model output, without applying any observation-based delta change method.

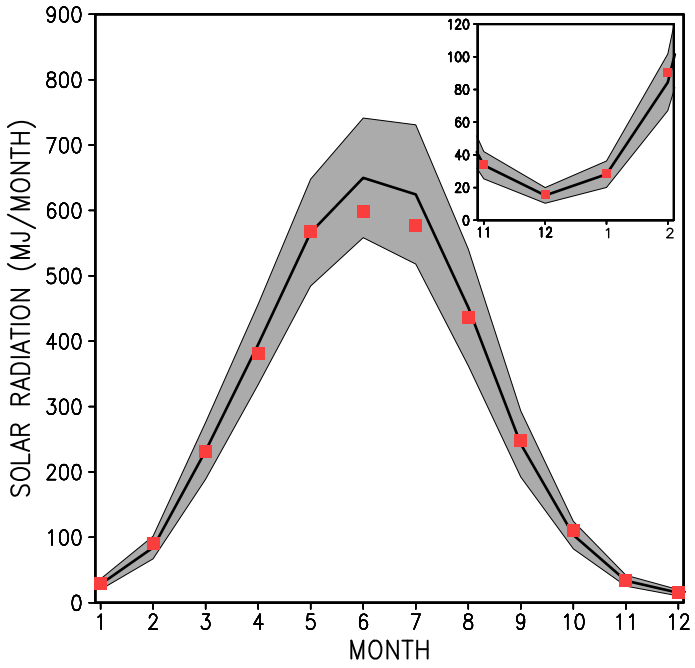

Fig. 1. Comparison of the modelled incident solar radiation with observations. Red squares: the baseline period (1971-2000) mean of the global radiation observed at Jokioinen in southwestern Finland (60.8°N, 23.5°E) for each calendar month. The thick black curve: the corresponding quantity as an average of the simulations performed with 18 global climate models. Grey shaded area: mean $\pm$ standard deviation of the simulations by the various models. In the large figure, months from January (1) to December (12) are depicted. On the right-top corner there is an enlarged illustration for November-February, i.e., the months with the weakest incident radiation. Unit: MJ m^{-2} month^{-1}.

analysis would corrupt the results severely. Therefore, the present analysis will be based on 18 models, with the CSIRO model excluded.

Evaluation of the quality of the model simulations was beyond the scope of this project, but a comparison between the modelled and observed radiation data was still performed for one example station. One can see that, for the baseline period, the mean of the 18 model simulation accords with observations surprisingly well (Fig. 1). In relative terms, the maximum deviations in the monthly values are of 8-9%, for several months less than 2%. The good accordance encourages utilization of the models to construct future projections. Admittedly, there is quite a large scatter among the various models, and consequently one is more justified to base the projections on the entire ensemble of the models rather than on any individual model.

2 ESTABLISHMENT OF THE PROJECTIONS

The output of the model simulations was represented on the native grids of each individual model. Therefore, the monthly means of the modelled radiation were first interpolated onto a common 2.5 x 2.5 degree grid, and 30 year running means were applied to smooth the influence of random interannual variability. Thereafter, anomalies from the baseline period mean were calculated.

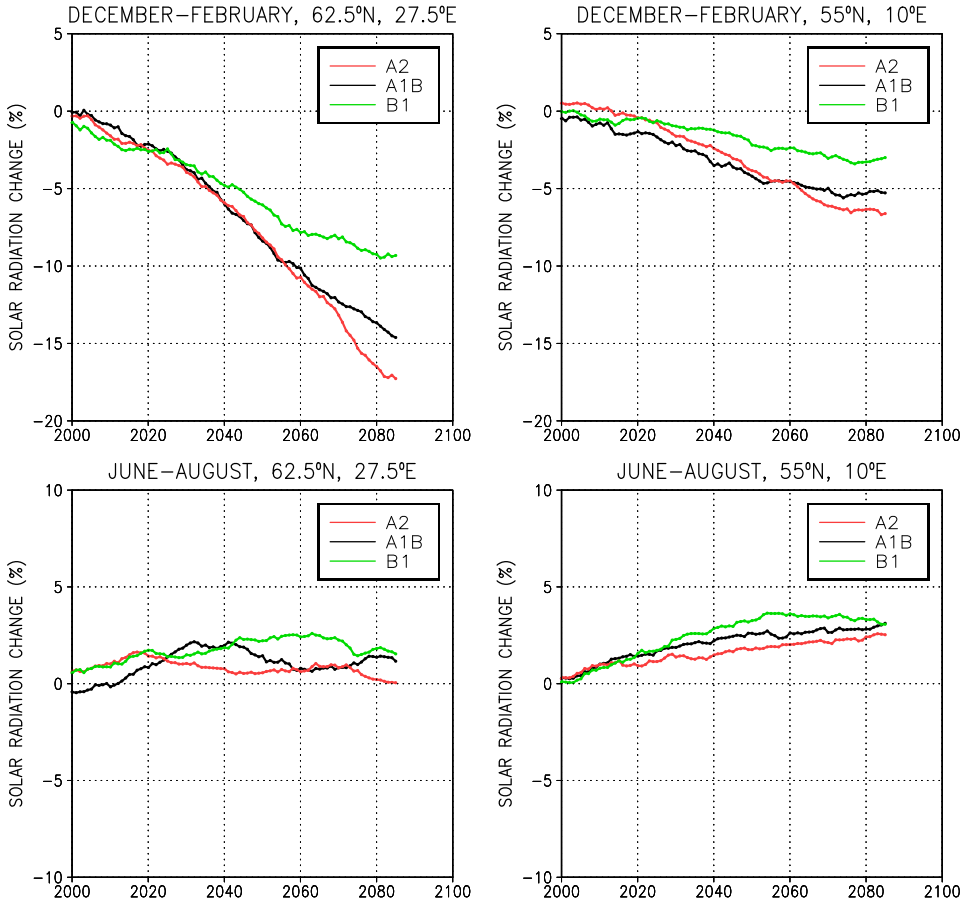

Fig. 2. Percentage change of incident global solar radiation for years 2000-2085, relative to the baseline period 1971-2000 mean. Left panels: south-eastern Finland (62.5°N, 27.5°E); right panels: southern Denmark (55°N, 10°E). The upper row shows time series for winter, the lower row for summer; note the different scale for the two seasons. The curves represent 30-year running means of the 18-model mean change, separately for the A2 (red), A1B (black) and B1 (green) greenhouse gas scenarios.

An unweighted mean of the responses simulated by the 18 models was used to give the best-estimate projection. To construct the probability distribution for the change, a normal distribution was fitted to the projections simulated by the various models and percentage points were determined from this distribution. Both the best estimate projection and the probability distribution were calculated separately for the three greenhouse gas scenarios.

Before composing the probability distributions for individual calendar months, the standard deviations of the various model responses at monthly level were made commensurable with the corresponding deviations calculated from seasonal (3-month) means (Jylhä et al., 2008). This procedure does not have any impact on the best-estimate projections.

Time series of the projected change in incident solar radiation at two grid points are shown in Fig. 2; the corresponding time series for Iceland and Greenland are given in the appendix in Fig. A7. At the eastern Finland grid point, there is a marked decline in wintertime insolation. Before 2040, the responses to the three greenhouse gas scenarios are very similar, but by the end of the century the A2 scenario projects a decline nearly

twice as much as the B1 scenario (-17% vs. -9%). In the remaining three panels of Fig. 2, the radiation responses are fairly modest.

To conclude, during the period of the main interest for the present study, 2020-2049, the various greenhouse gas scenarios do not diverge much. The same conclusion was drawn by Räisänen and Ruosteenoja (2008, Fig. 7.3) in studying the temperature and precipitation responses. Therefore, in the main text we shall merely focus on the intermediate-level A1B scenario. In contrast, in the appendix all the three scenarios are included to demonstrate results for the end of this century.

3 BEST-ESTIMATE PROJECTIONS

The geographical distribution of the projected insolation change (an average of 18 models) is depicted in Figs. 3 (in percentage terms) and 4 (in absolute terms).

In the relative sense, largest changes occur in winter in central Scandinavia and southern Finland, where more than 5% of incident radiation would be lost (Fig. 3(a)). According to the t test, the signal is statistically significant at the 1% level. Over the Barents Sea, the decline is even larger, but this is evidently an artifact of the model data set. In several models, the simulated present-day climate is too cold, and the Barents Sea is thus erro-

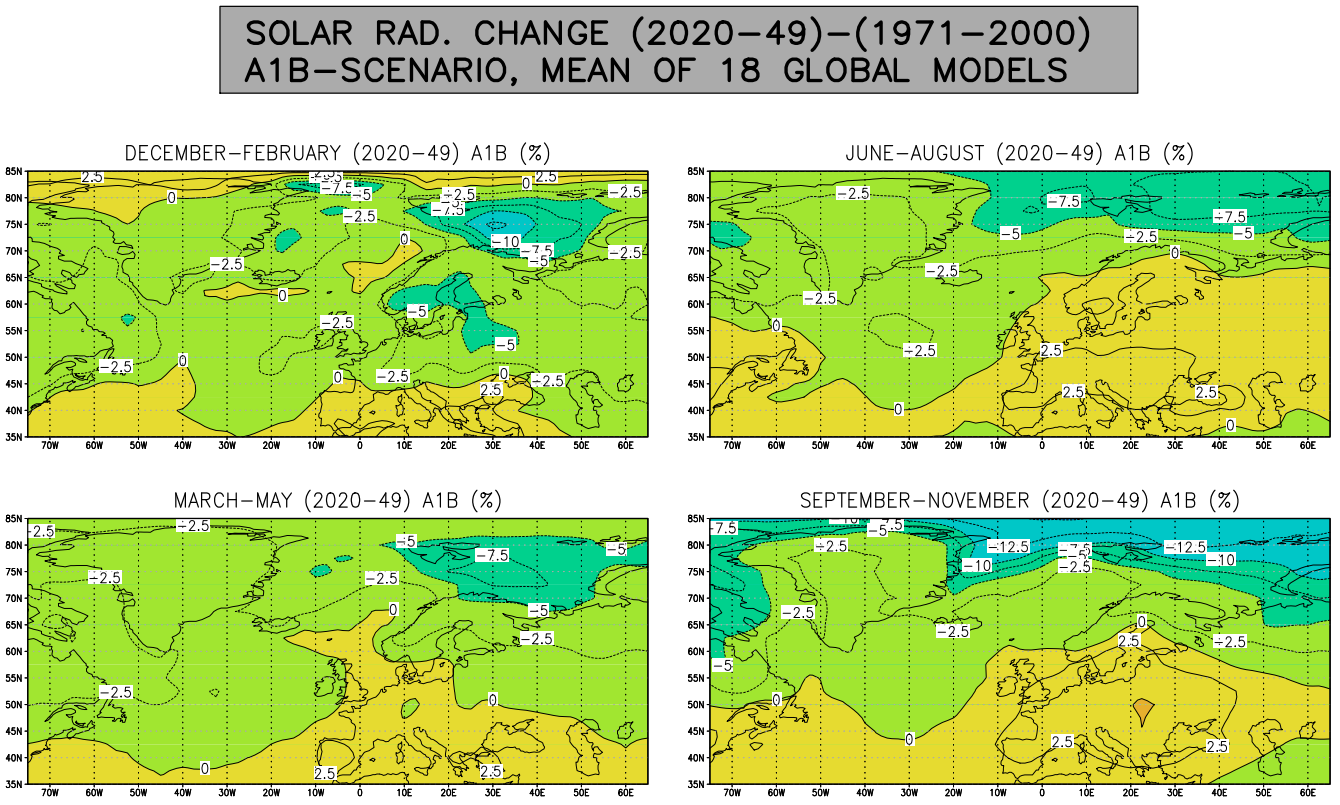

Fig. 3. Percentage change in the incident solar radiation from period 1971-2000 to 2020-2049 under the A1B greenhouse gas scenario; a mean of the simulations performed with 18 global models. Top-left: winter, bottom-left: spring; top-right: summer; bottom-right: autumn.

neously covered by ice in winter. Multiple scattering between the cloud cover and the high-albedo surface enhances the simulated insolation significantly. During the simulation, the ice disappears and, accordingly, incident radiation is simulated to decrease.

In the remaining three seasons, changes are quite modest, less than $\pm$ 5% almost everywhere with the exception of high-latitude sea areas. In summer and autumn, large areas in Scandinavia experience a slight increase in the insolation, but this increase is not statistically significant apart from in places in southern Scandinavia.

When the radiation response is studied in absolute terms (Fig. 4), the impression becomes somewhat different. In the winter months, changes in Nordic areas are very minor, less than 10 MJ m^{-2}. This also holds for autumn, apart from southern Scandinavia where insolation increases by 10-20 MJ m^{-2}. The largest changes occur in spring and summer, with the maximum decreases (increases) of the order of 40 MJ m^{-2} taking place in northern Lapland in spring (southern central Sweden in summer). Note also the substantial decrease in Greenland in summer, 40-60 MJ m^{-2}. In places over the Arctic ocean, more than 100 MJ m^{-2} of insolation is lost in summer. One explanation for this is the decreasing sea ice extent, accompanied by a disappearance of multiple scattering of shortwave radiation (see discussion above).

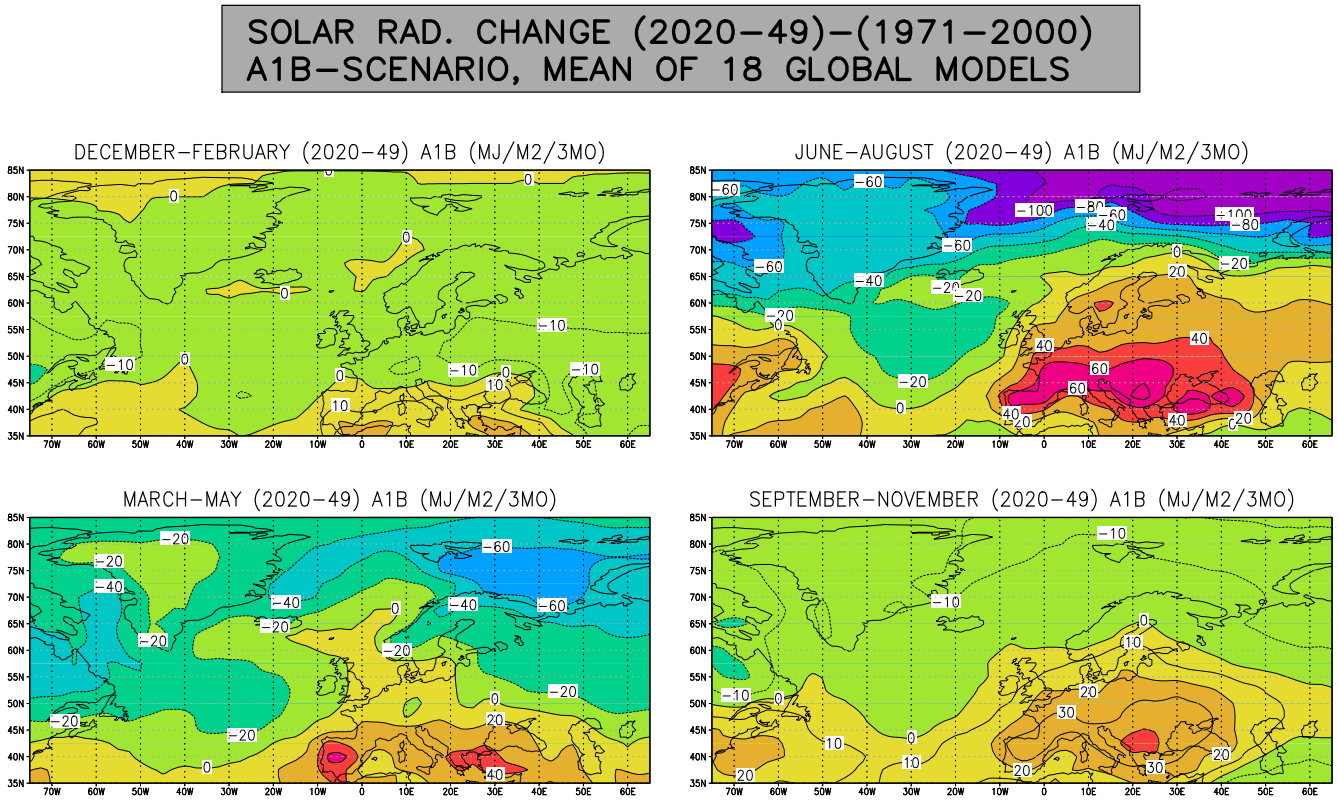

Fig. 4. As Fig. 3, but the change presented in absolute terms (MJ m^{-2} within the 3-month period). In the panels for winter and autumn, contour interval is 10 MJ m^{-2}, for spring and summer 20 MJ m^{-2}. The colour scale is the same in all panels.

In southern and (except for winter) central Europe solar radiation conditions are simulated to become more favourable. There are areas where the annual insolation increases by more than 100 MJ m^{-2}.

Albeit that task was not contained in the original research plan, we also calculated insolation responses for a more distant period, 2070-2099. Maps for that period are presented in the appendix (Figs. A1-A6). Qualitatively, the geographical distributions are similar to those for the period 2020-2049 but the amplitude of the response is stronger, the A2 scenario producing the strongest, the B1 scenario the weakest response.

4 UNCERTAINTY ANALYSIS

Probability distributions for the insolation change, separately for each calendar month at four grid points, are depicted in Fig. 5. There are a number of cases in which the probability of the change exceeds 75% or even 90%. Among these, the decline of insolation in eastern Finland (Fig. 5(d)) in April and November appears to have the highest probability.

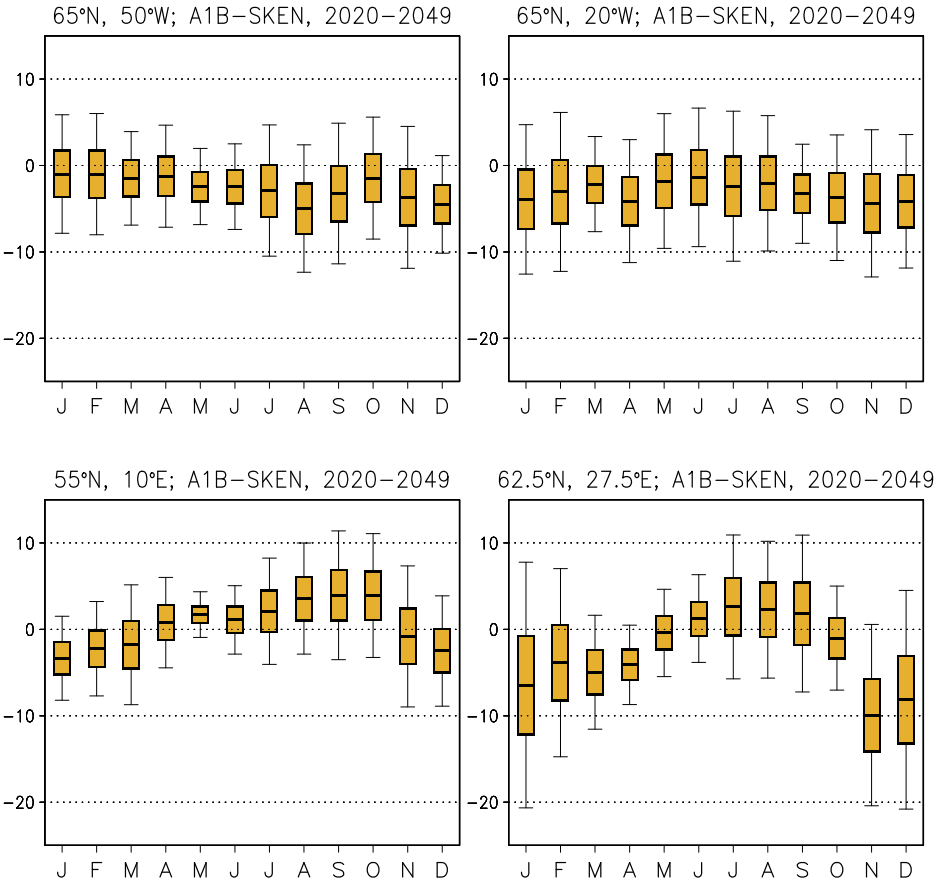

Fig. 5. Monthly probability distributions for the percentage change of incident solar radiation from the period 1971-2000 to 2020-2049 under the A1B greenhouse gas scenario, derived from simulations performed with 18 global models. The yellow box covers the interval between the 25th and 75th percentage points, with the median (50th point) shown by a black line. Whiskers represent the interval from the 5th to the 95th percentage point. Top-left: south-western Greenland (65°N, 50°W); top-right: central Iceland (65°N, 20°W); bottom-left: southern Denmark (55°N, 10°E); bottom-right: south-eastern Finland (62.5°N, 27.5°E).

The robustness of the response increases as the climatic warming proceeds. This can be seen from Fig. A8 in the appendix, where probability distributions are given for the period 2070-2099. For example, at that stage in eastern Finland the probability of insolation decline exceeds 95% in three months.

5 CONCLUSIONS

- In relative terms, the largest change projected to take place is a decline of insolation in the Nordic area in winter. In absolute terms, this decline is not large, but may have influence on the need for energy in illumination.
- In the other seasons, percentage changes are relatively modest. Roughly speaking, the more southern the location, the more positive insolation changes can be expected.
- In Iceland and Greenland, insolation seems to decrease by a few percents in all seasons.
- As far as solar energy production is concerned, the wintertime decrease in insolation in northern Europe is evidently of minor importance, since in the dark season conditions for this method of energy production are unfavourable in any case. In summer and early autumn the conditions will improve slightly, chiefly in southern Scandinavia. Nonetheless, the marked enhancement of insolation in central and southern Europe may prove to be more important, affecting the competitive ability of the various parts of Europe on the solar energy market.
- Projected changes in solar radiation and precipitation in Europe seem to be generally opposite: a drier and sunnier climate in the south, a wetter and darker climate in the north. Accordingly, changes in the conditions of solar and hydropower energy production are compensatory. At present, of course, the rôle of solar energy is negligible compared to hydropower production, but the status may alter in the future.

REFERENCES

Jylhä K., Ruosteenoja K., Räisänen J., Venäläinen A., Tuomenvirta H., Ruokolainen L., Saku S. and Seitola T., 2009: Arvioita Suomen muuttuvasta ilmastosta sopeutumistutkimuksia varten. ACCLIM-hankkeen raportti 2009. (Changing climate in Finland: estimates for adaptation studies. ACCLIM project report 2009). Finnish Meteorological Institute, *Report* **2009:4**. (In Finnish, extended abstract in Swedish and English)

Ruosteenoja, K., Tuomenvirta, H. and Jylhä, K., 2007: GCM-based regional temperature and precipitation change estimates for Europe under four SRES scenarios applying a super-ensemble pattern-scaling method. *Clim. Change*, **81**, 193-208.

Räisänen, J. and K. Ruosteenoja, 2008: Probabilistic forecasts of temperature and precipitation change based on global climate model simulations. CES deliverable 2.2, 46 pp. Available from http://www.atm.helsinki.fi/ ~jaraisan/CES_D2.2/CES_D2.2.html

APPENDIX

(A) MAPS FOR THE PERIOD 2070-2099

Although this period is beyond the principal scope of the CES project, the information is useful for several reasons: the responses are stronger and more significant statistically than those for the early-mid century; the influence of greenhouse gas emissions becomes clearly discernible, etc.

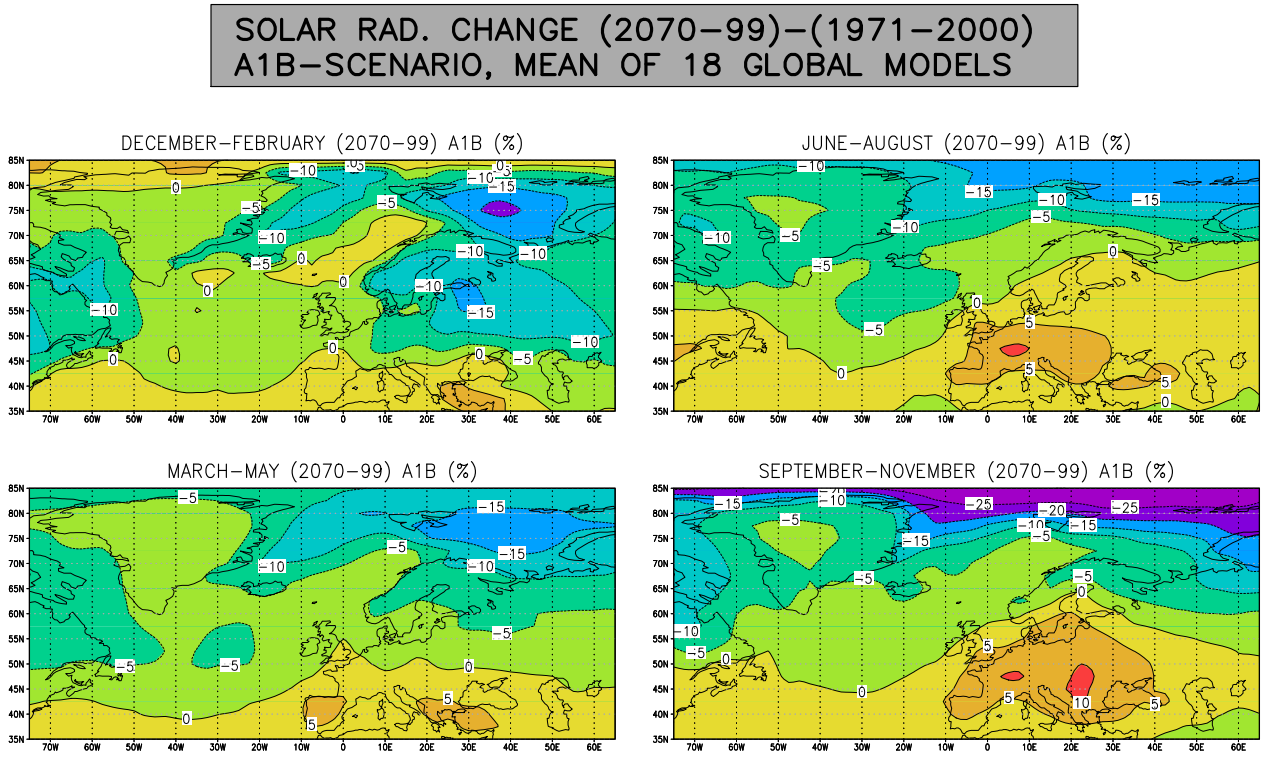

Fig. A1. Percentage change in the incident solar radiation from period 1971-2000 to 2070-2099 under the A1B greenhouse gas scenario; the mean of simulations performed with 18 global models. Top-left: winter, bottom-left: spring; top-right: summer; bottom-right: autumn.

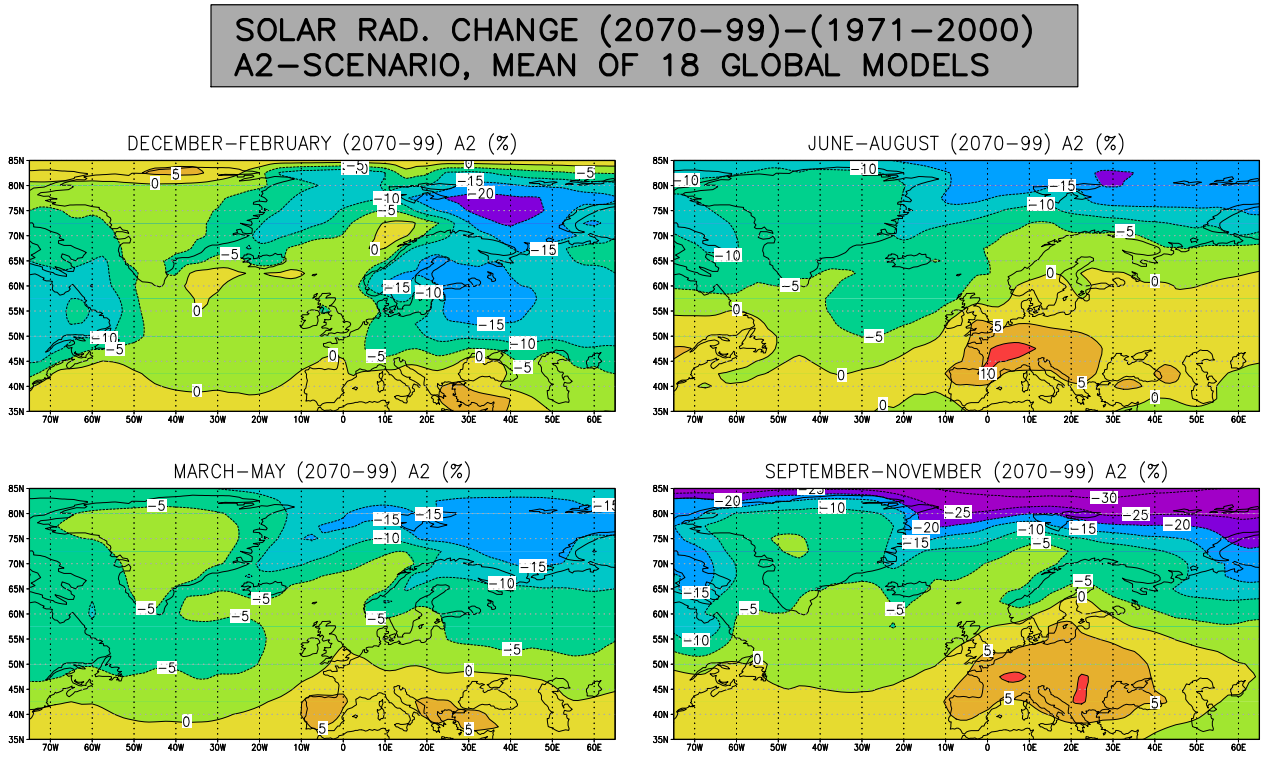

Fig. A2. As Fig. A1, but for the A2 scenario.

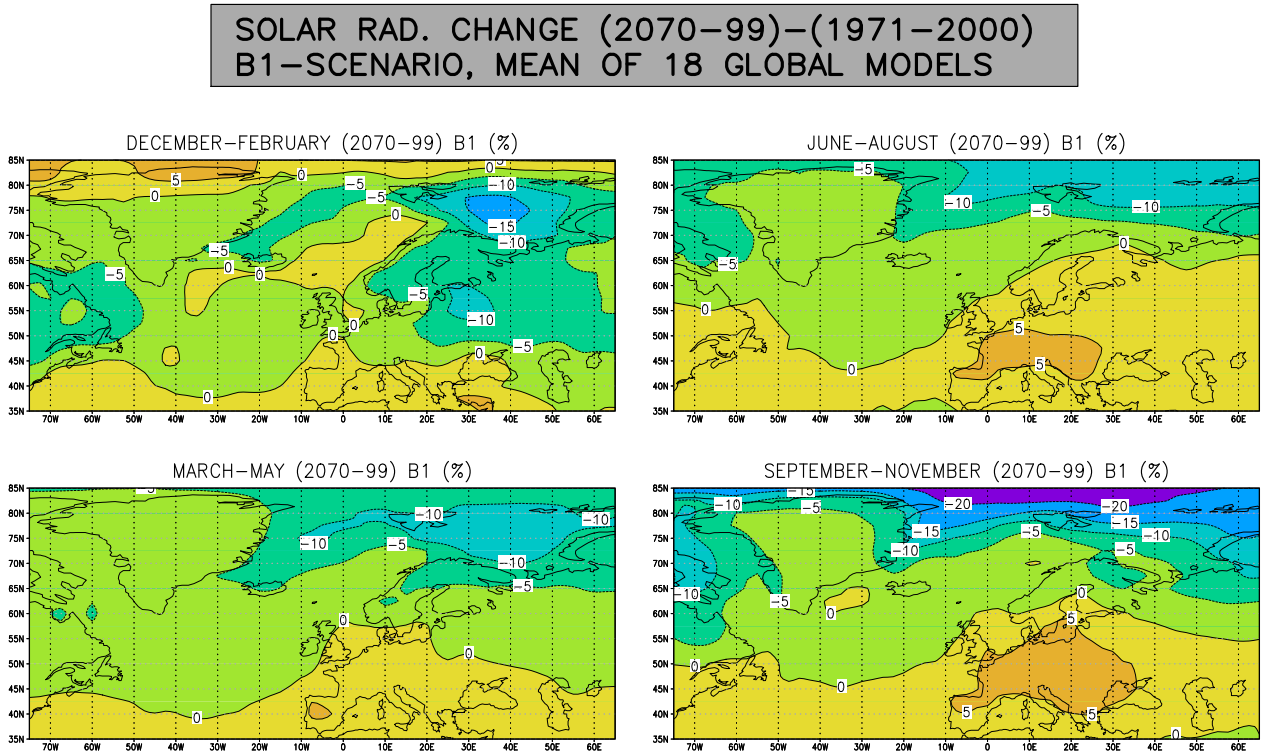

Fig. A3. As Fig. A1, but for the B1 scenario.

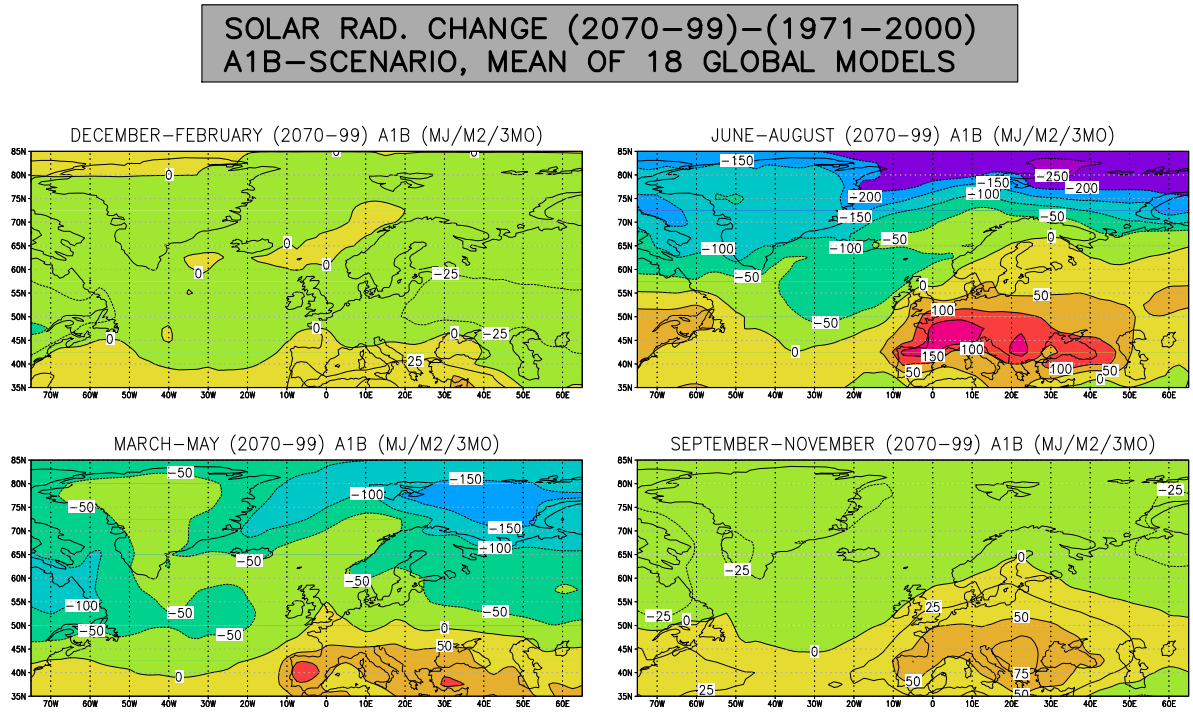

Fig. A4. As Fig. A1, but the absolute change of insolation under the A1B scenario. In the panels for winter and autumn, contour interval is 25 MJ m^{-2}, in those for spring and summer 50 MJ m^{-2}. The colour scale is the same in all panels.

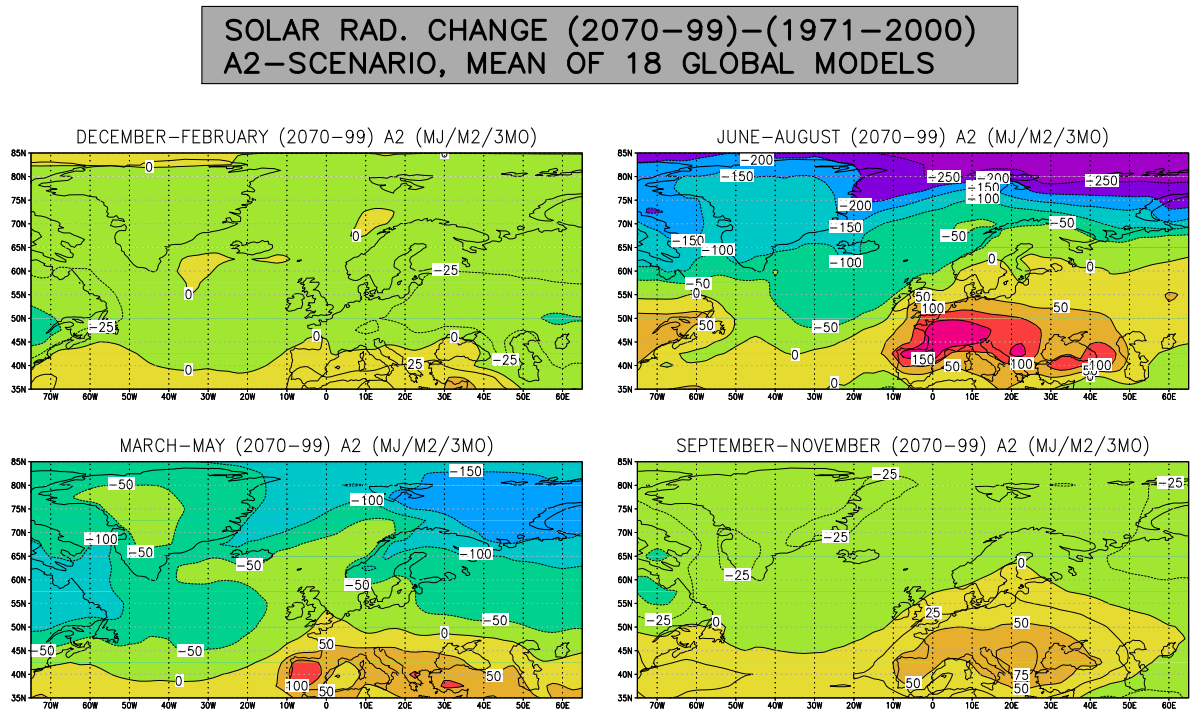

Fig. A5. The absolute insolation change under the A2 scenario.

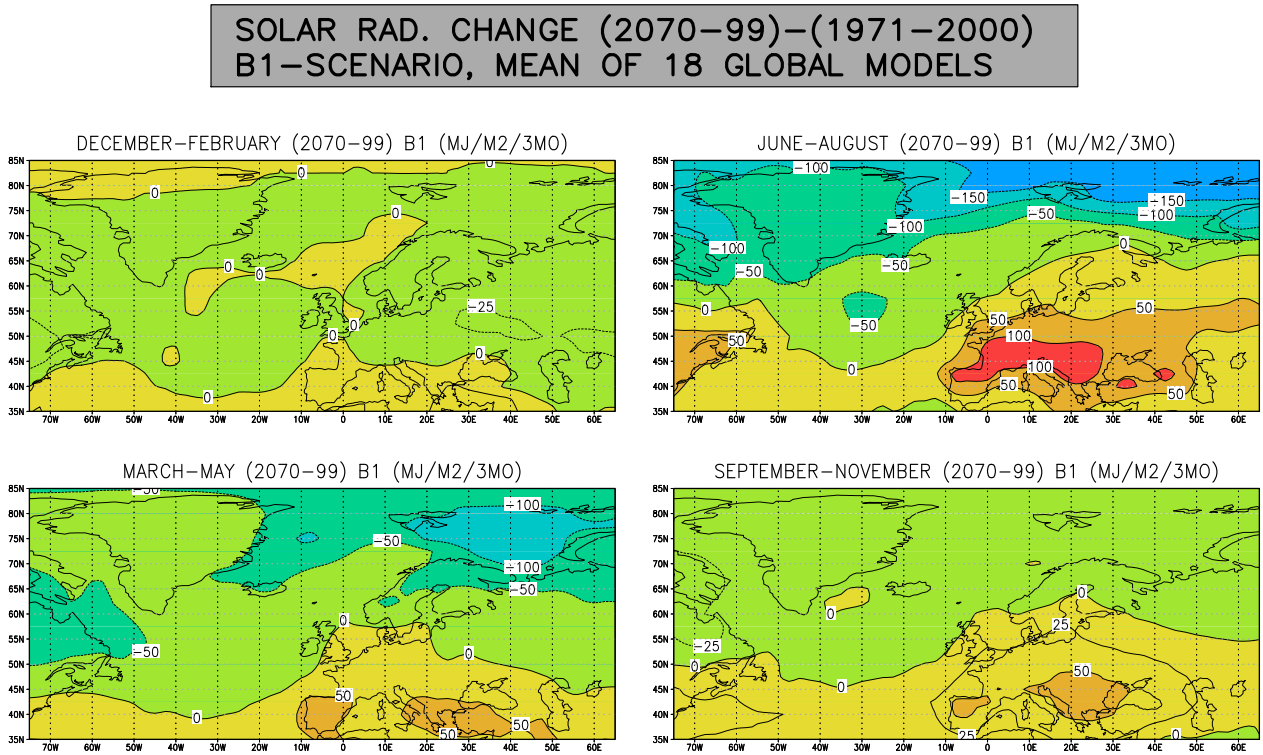

Fig. A6. The absolute insolation change under the B1 scenario.

(B) TIME SERIES

Fig. A7 shows the time series of seasonal changes in incident radiation for Greenland and Iceland.

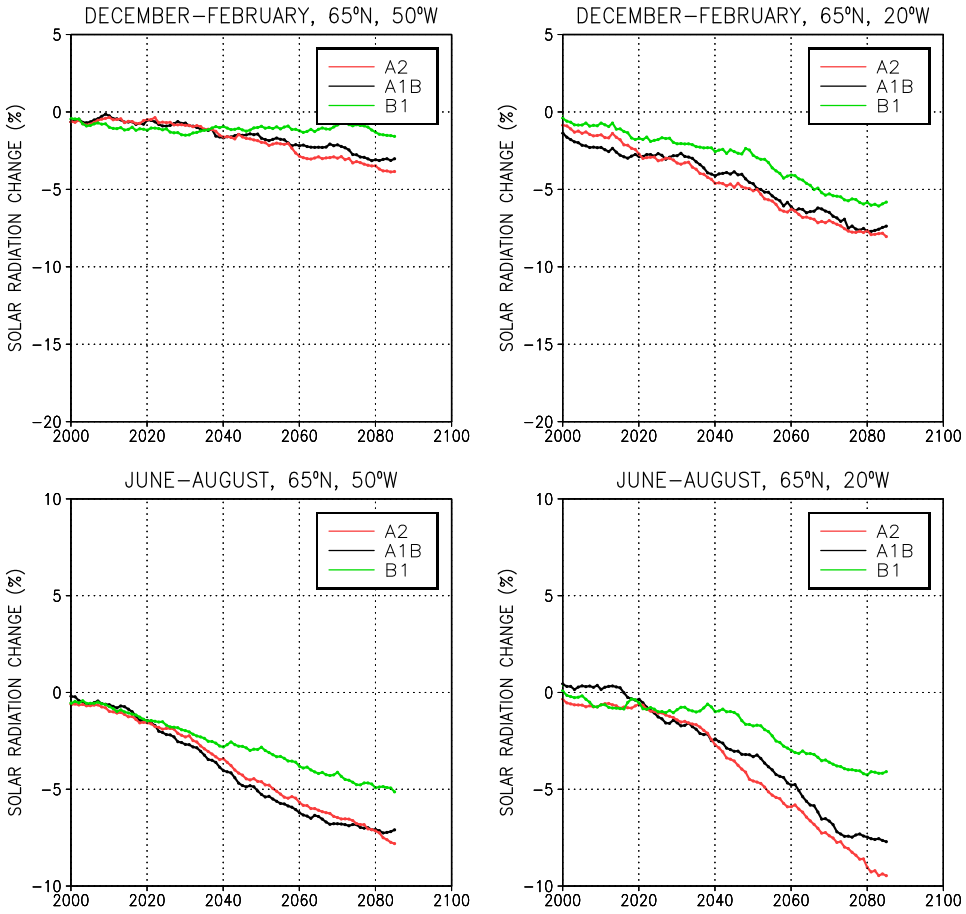

Fig. A7. Percentage change of incident global solar radiation for years 2000-2085, relative to the baseline period 1971-2000 mean. Left panels: southwestern Greenland (65°N, 50°W); right panels: central Iceland (65°N, 20°W). The upper row shows time series for winter, the lower row for summer. The curves represent 30-year running means of the 18-model mean change, separately for the A2 (red), A1B (black) and B1 (green) greenhouse gas scenarios.

(C) PROBABILITY DISTRIBUTIONS FOR THE END OF THE CENTURY

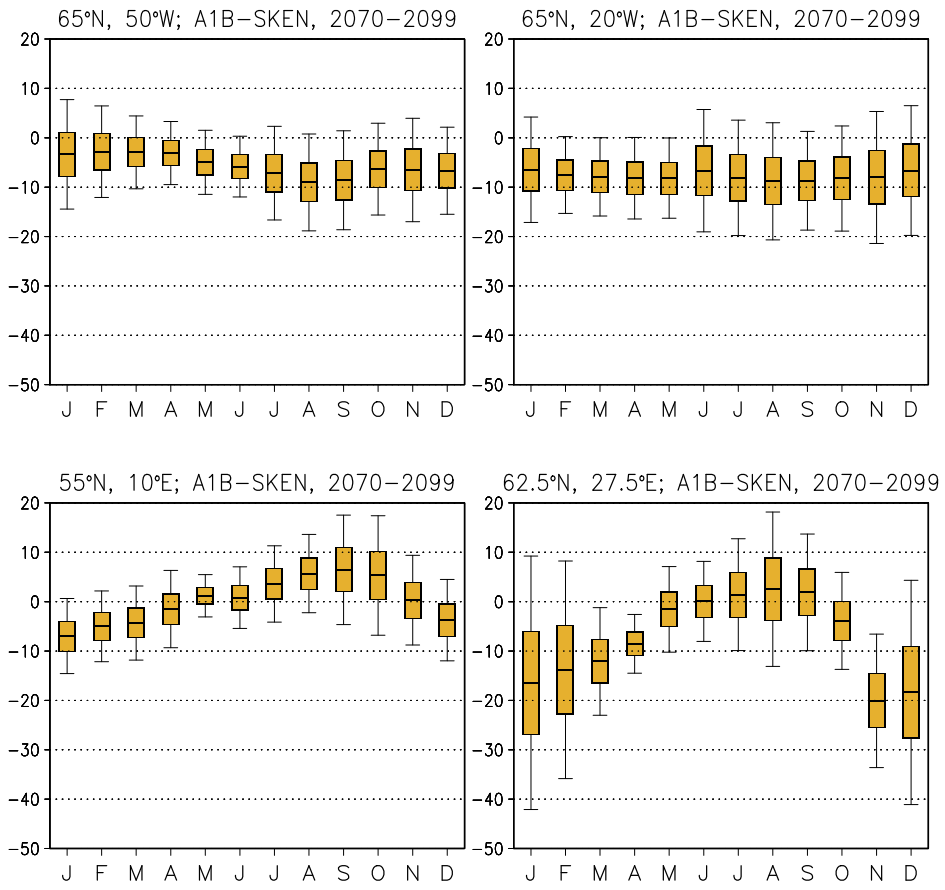

Fig. A8. Monthly probability distribution for the percentage change of incident solar radiation from the period 1971-2000 to 2070-2099 under the A1B greenhouse gas scenario, derived from simulations performed with 18 global models. The yellow box covers the interval between the 25th and 75th percentage points, with the median (50th point) shown by a black line. Whiskers represent the interval from the 5th to the 95th percentage point. Top-left: south-western Greenland (65°N, 50°W); top-right: central Iceland (65°N, 20°W); bottom-left: southern Denmark (55°N, 10°E); bottom-right: south-eastern Finland (62.5°N, 27.5°E).